Polymer Bulletin (2019) 76:5701–5716
https://doi.org/10.1007/s00289-018-2657-7

ORIGINAL PAPER

# The comparative investigation on synthesis, characterizations of silver ion-imprinting and non-imprinting cryogels, their impedance spectroscopies and relaxation mechanisms

**Koray Şarkaya**[1,3] · **Ahmet Demir**[2]

Received: 14 August 2018 / Revised: 6 December 2018 / Accepted: 10 December 2018 /
Published online: 11 January 2019


## Abstract

In the present study, a novel ion-imprinting and non-imprinting cryogel samples have been prepared using ion-imprinting technique and the dielectric properties have been investigated using an impedance spectroscopy method. In the preparation of ion-imprinted cryogel, at the first attempt, *N*-methacryloly-(L)-cysteine methyl ester was used as the metal complexing monomer. $Ag^{+}$-imprinted poly(hydroxyethyl methacrylate-*N*-methacryloly-(L)-cysteine methyl ester) cryogel was produced by bulk polymerization. Poly(2-hydroxyethyl methacrylate) was selected as the basic matrix by considering properties, high chemical and mechanical stability. After removal of template (silver ions), the ion-imprinted cryogel was used for the removal of photo-film-containing materials. The dielectric properties of cryogel samples have also been investigated by impedance spectroscopy within the frequency range of 1 Hz–10 MHz. The real part of the permittivity increases at low frequencies as electrode effects become dominant. It shows a constant value at high frequencies due to dipole polarization. On the other hand, the imaginary part does not show a relaxation peak as the relaxation time of samples is very short. The frequency dependence of electrical modulus has also been investigated. The real part of electrical modulus ($M'$ ($f$)) is an indicative of negligible electrode polarization phenomenon in the test material. The behavior of the imaginary part of frequency dependent electrical modulus ($M''$ ($f$)) exhibit that the dielectric relaxation process is usually not frequency-activated state. Dielectric relaxation process occurs spontaneously due to the hopping mechanism of charge carriers.

**Electronic supplementary material** The online version of this article (https://doi.org/10.1007/s00289-018-2657-7) contains supplementary material, which is available to authorized users.

✉ Koray Şarkaya
koraysarkaya@duzce.edu.tr

Extended author information available on the last page of the article

**Keywords** Cryogel · *N*-Methacryloly-(L)-cysteine methyl ester · Ion-imprinting · Molecular imprinting · Polymers · Dielectric properties · Electrical modulus

## Introduction

Molecular imprinting is a very suitable technique in the creation of recognition sites in a macromolecular matrix with the use of a template molecule [1]. For this aim, the template molecule is linked with selected functional monomers, and then, the resulting complex turns out to be a solid matrix using the cross-linking agent [2, 3]. The result of polymerization generates a macromolecular matrix that consolidates the performed interaction network. The polymer has high affinity and specify on its structure after the removal of template agent leaving behind cavities in the molecule [4]. Due to some advantages of the molecularly imprinted polymers (MIP)'s such as being economical, ease in preparation, decisiveness and high potential in molecular recognition, MIPs should be accepted as artificial affinity media [5]. In chemistry field, molecular recognition-based separation and characterization techniques have popularity thanks to their selection potential with regard to the molecules targeted. The technique is widely applied efficiently for imprinting some of the small biomolecules such as amino acids, proteins and metal ions [6–18]. At this point, the application of polymeric materials in some techniques including adsorption and purification of biomolecules in biotechnology has gained more attention recently. Also, these polymeric materials are easy to be applied for applications of purification and separation of biological molecules, as the most important aspect. Using these polymers in biotechnology allows continuous improvement in the process of techniques for biomolecules [19]. Recently, the application of gels as polymeric materials based on polymer chemistry contributes to the application of polymeric materials for use in biotechnological activities [20]. Cryogels are supermacroporous hydrogels used as monoliths or chromatographic columns, which could be held by radicalic polymerization of monomers under zero degrees [21, 22]. Cryogels also ensure suitability when they are used together with viscous media such as metal ions-containing wastewater. Since cryogels could be shaped in different sizes and templates like disks, sheets or monoliths with different formations, they have advantages over polymers. It is the interconnected macroporous structure of cryogels that renders appropriateness for various applications [23–27].

One of the applications of molecular imprinting method, ion-imprinting technology, has become increasingly popular. It is through this method that metal ions can be imprinted or embedded on polymer matrix and the molecule can gain affinity for these ions [28].

Ion-imprinting method requires three steps: (1) complexation of template (i.e., metal ions) to a polymerizable ligand, (2) polymerization of this complex, (3) removal of template following polymerization. The characteristics of ligand, the coordination geometry and coordination number of the ions as well as their charge and size are determinate in the selection quality of polymeric adsorbent [29–34]. Also in literature, it is well reported that $Ag^+$ ions reduce to silver nanoparticles through the dissolved functional polymers. It can be seen that reduced silver nanoparticles usually exhibit SPR peaks at the visible region [35–44].

One of the advantages of using molecularly imprinted polymers is that they are readily available, cheap and easily prepared. Another advantage of molecular imprinted polymers is that they contain high mechanical properties due to their resistance to heat and pressure. These molecules are highly resistant polymeric materials due to their high stability in environments containing acidic or basic, metal ions or organic solvents. They continue to be practicable for several years without disrupting their performance [12–16]. Eventually, molecularly imprinted polymers are used because of their selective advantage in chromatographic processes, so in view of the advantages of molecularly imprinted polymers, ion-imprinting method which is one of the most suitable methods for selective behavior in chromatographic applications is preferred. The focus point of this investigation is to manifest the differences between the structural features and relaxation mechanisms of both silver-imprinted and non-imprinted cryogels. For this aim at first, we have prepared the silver ion-imprinted and non-imprinted cryogel using ion-imprinting technique and the structures of the molecules have been characterized using elemental analysis (EDAX), Fourier transform infrared spectroscopy (FT-IR) and scanning electron microscope (SEM). Then, the impedance spectroscopies of the prepared samples were investigated using a Novocontrol Alpha-A Impedance Analyzer ranging from 1 Hz to 10 MHz at room temperature in the air ambient and under total darkness.

## Experimental

### Materials

The functional monomer *N*-methacryloyl-L-cysteine methyl ester (MAC) was obtained from NANOREG (Ankara, Turkey). 2-Hydroxyethyl methacrylate (HEMA), cross-linkers, ethylene glycol dimethacrylate (EGDMA) and *N*,*N*′-methylenebis(acrylamide) (MBAAm), and initiators, azobis(isobutyronitrile) (AIBN) and ammonium persulfate (APS), and the redox couple *N*,*N*,*N*′,*N*′-tetramethylethylenediamine (TEMED) were obtained from Sigma-Aldrich Chem. Co. (St. Louis, MO). The remaining chemicals and equipments, whether or not mentioned here, had reagent grade and were purchased from Merck AG (Darmstadt, Germany) or local distributors. It was through a Barnstead (Dubuque, IA) ROpure LP® that the water in the adsorption experiments was distilled with reverse osmosis unit which had a high flow cellulose acetate membrane (Barnstead D2731), with Barnstead D3804NANOpure® for organic/colloid removal and ion exchange packed-bed system used as the second process.

### Preparation of $Ag^+$–MAC complex

In the preparation of MAC–$Ag^+$ complex, 15 ml of ethanol–water mixture (50/50 v/v) was slowly added to solid *N*-methacryloly-(L)-cysteine methyl ester (MAC) (0.189 g, 1.0 mmol) followed by treatment with silver nitrate ($Ag(NO_3)$) (0.169 g, 1.0 mmol) at room temperature with constant stirring for 2 h. Afterward, a filtration process was applied on the metal–monomer complex, the washing and drying

process of which was performed with 99% ethanol (250 ml), and vacuum oven, respectively. The molecular formulas of the functional monomer and the complexation between MAC and $Ag^+$ are shown in Fig. 1a, b, in order.

### Preparation of PHEMAC-$Ag^+$ cryogel

In order to prepare PHEMAC-$Ag^+$ cryogel, first, deionized water was used to dissolve monomers (1.3 ml HEMA, 10 ml *N*,*N*-methylenebis(acrylamide) (MBAAm), 1 ml MAC/$Ag^+$), and the elimination of soluble oxygen was made possible by degassing the mixture under vacuum for about 5 min. Total concentration of monomers was 10% (w/v). With the radicalic polymerization process, including *N*,*N*,*N*,*N*-tetramethylene diamine (TEMED, 25 l) and ammonium persulfate (APS, 20 mg), the cryogel was synthesized. The cooling process of the solution was performed in ice bath in a time span of 2 or 3 min following the application of APS. It was only after the application of TEMED that the stirring process of the mixture was completed. This process was followed by the addition of the mixture into the plastic syringe (5 ml 0.8 cm). After the reaction mixture's treatment in plastic syringe, the polymerization solution was cooled under − 12 °C for 12 h, at least. The following day, the produced cryogel was washed by some distilled water, followed by the storage of cryogel in buffer with 0.02% sodium azide at 4 °C till application. For the removal of some contamination reagents, monomers or porogenic diluents, we used chromatographic system, which is attached with plastic syringe that consumed polymerization solution, and also this system allowed to pump ethyl alcohol and water at a flow rate of 1.0 ml/min, respectively. For the removal of $Ag^+$ ions, which is templated in porouses of cryogel (PHEMAC-$Ag^+$), we used 0.25 M EDTA solution, which is one of the best available sources for the removal of the metal ions with coupling [14]. The chromatographic system pumped 0.25 M EDTA solution to $Ag^+$-imprinted cryogel column for hours. After the removal of silver ions from the cryogel totally, (PHEMAC-$Ag^+$) was eventually rinsed with 0.1M $HNO_3$. The

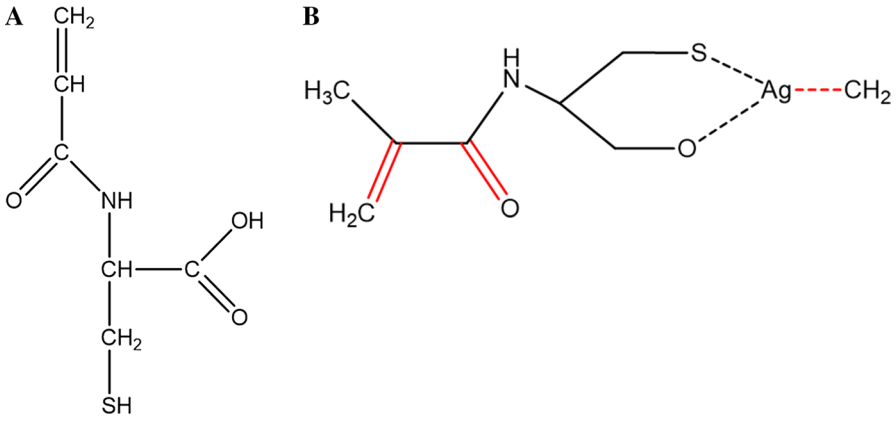


**Fig. 1** **a** Molecular formula of MAC (*N*-methacryloly-(L)-cysteine methyl ester), **b** possible molecular formula of MAC–$Ag^+$ complex

obtained PHEMAC-$Ag^+$ was kept at 4 °C till application. We also synthesized non-imprinted cryogel (PHEMAC) to use as a view to comparison. This was carried out with the same polymerization procedure applied on PHEMAC-$Ag^+$, but this was not used with the template silver ions that were applied in the preparation of PHEMAC-$Ag^+$ at this time.

### Preparation of cryogel samples for impedance measurements

Both imprinting and non-imprinting cryogel samples were prepared using Shimadzu Rotary Vacuum Pump for pellet obtaining at room temperature in the air ambient. The diameters of the prepared samples were measured as 9 mm, and their thickness was measured as 1 mm with digital calipers. Then, the impedance spectroscopies of the prepared samples were investigated using a Novocontrol Alpha-A Impedance Analyzer ranging from 1 Hz to 10 MHz at room temperature in the air ambient and under total darkness.

## Results and discussions

### Chemical analyses

#### FT-IR analysis

The overlapped FT-IR spectra of the silver ion-imprinted supermacroporous poly(hydroxyethyl methacrylate)-based cryogel and non-imprinted cryogel molecules are presented in Fig. 2. As shown in Fig. 2, FT-IR spectra of poly(HEMA-MAC) have a broad peak at 3344.87 $cm^{-1}$ that consists of several sharp peaks as the stretching vibration bands of hydrogen-bonded alcohol (HEMA). The characteristic amide I and amide II absorption bands can be seen at 1652.70 and 1530.13 $cm^{-1}$, respectively. In addition, strong carbonyl stretching vibration at around 1724.13

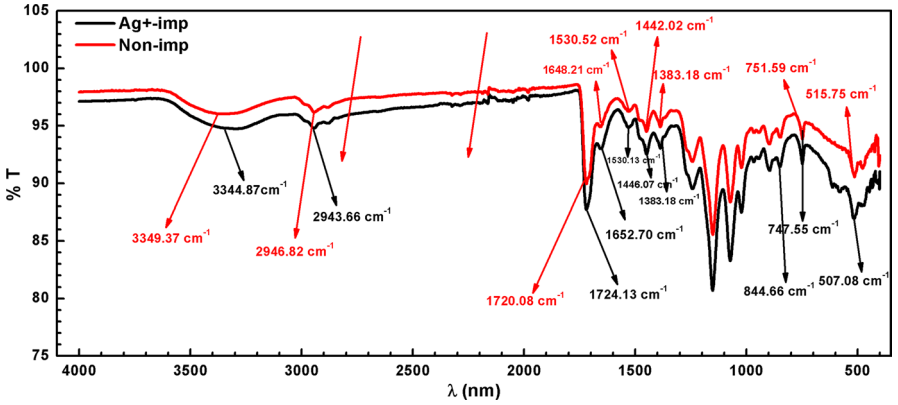


**Fig. 2** **a** FT-IR spectrum of $Ag^+$-imprinted cryogel, **b** FT-IR spectrum of non-imprinted cryogel

**Fig. 3** **a** Elemental analysis of $Ag^+$-imprinted poly(hydroxyethyl methacrylate) (PHEMA)-based cryogels, **b** elemental analysis of $Ag^+$-imprinted poly(hydroxyethyl methacrylate) (PHEMA)-based **c** SEM photographs of non-imprinted cryogels, **d** SEM photographs of $Ag^+$-imprinted cryogels **e** element mapping of non-imprinted cryogels, **f** element mapping of $Ag^+$-imprinted cryogels ▶

$cm^{-1}$ and C–O stretching vibrations at 1250.8 $cm^{-1}$ were observed. In order to identify the functional properties of complex, on grounds of linear coordinate covalent complex formation, the specific S–H stretching vibration bands at 907 $cm^{-1}$ and 849 $cm^{-1}$ slip to the higher-frequency field at 844.66 $cm^{-1}$ and 747.55 $cm^{-1}$ because of a reduction in electron density of sulfhydryl group of MAC monomer. The characteristic S–H bonds are observed between 2550 $cm^{-1}$ and 2600 $cm^{-1}$. The S–H bending peak appears at 2625 $cm^{-1}$ of MAC [45]. For the characteristic determination of complex, due to linear coordinate covalent complex formation, the S–H bending peak at 2625 $cm^{-1}$ slips to higher wavelength at 2943.66 $cm^{-1}$ because the chemical bond formed between the silver and sulfur groups due to the coordinated covalent bond structure is harder and more rigid. Also, Fig. 2 exhibits that the non-imprinted cryogel has almost similar characteristic behaviors with silver ion-imprinted cryogel, except S–H vibration bands.

## Elemental and SEM analysis

The results of elemental analysis for non-imprinted and silver ion-imprinted poly(hydroxyethyl methacrylate) (PHEMA)-based cryogels are presented in Fig. 3a, b, respectively. One of the most important findings of the results of the elemental analysis was to determine the presence of the MAC co-monomer in both cryogels. With the detection of sulfur groups, the presence of MAC co-monomer is proved. Due to the fact that it is possible to make covalent bonding with template molecules through sulfur groups, MAC monomer is preferred as functional monomer as metal complexing monomer in our study. Another finding we obtained from the results of the elemental analysis is that silver ions were expected to be observed in silver ion-imprinted cryogel and silver ions were not found in non-imprinted cryogel. 0.001485 mol MAC/g polymer was confirmed as total equivalent amount of functional monomer in the polymer structure.

The morphology of the non-imprinted and $Ag^+$ ion-imprinted cryogels was examined with scanning electron microscopy (SEM). Figure 3c, d shows SEM photographs of $Ag^+$-imprinted and non-imprinted cryogels. The groups in the macroporous polymeric structure were symbolized by element mapping method, which is shown in Fig. 3e, f, and the findings were strengthened in addition to the results obtained with elemental analysis. These cryogels were composed of interconnected cavities that form a macroporous structure. According to SEM photographs, the size of cavities was roughly determined in the range of 0.4–1.6 μm. Generally, the sizes of cavities of ion-imprinted cryogels were larger than non-imprinted cryogels.

During the preparation of cryogel, silver ion was used, which led to a change in polymerization kinetics. Unlike the conventional cryogel synthesis in which other metal ions rather than silver ion were used, the pores were more spherical and larger;

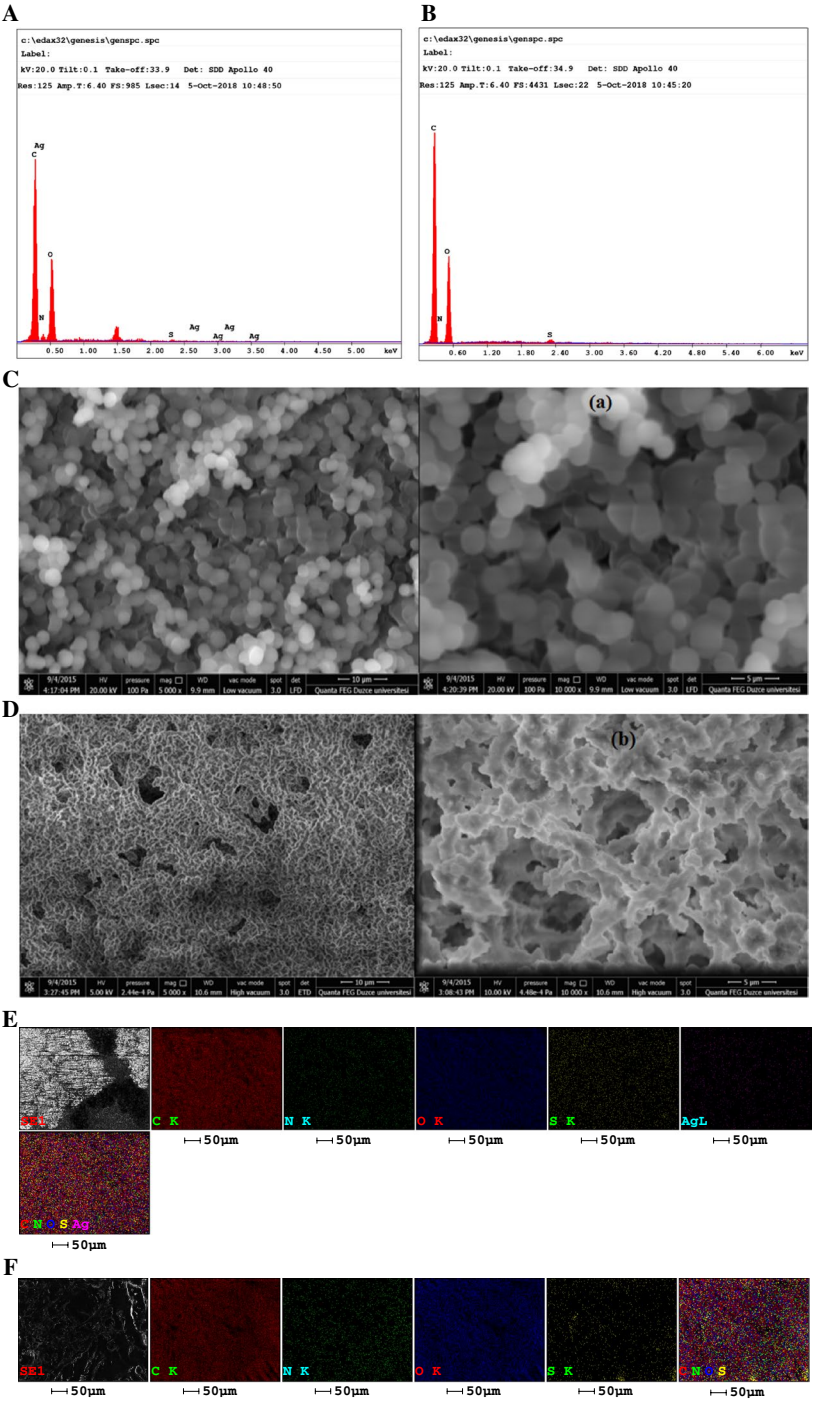
A
c:\edax32\genesis\genspc.spc
Label:
kV:20.0 Tilt:0.1 Take-off:33.9 Det: SDD Apollo 40
Res:125 Amp.T:6.40 FS:985 Lsec:14 5-Oct-2018 10:48:50
Ag
C
O
N
S
Ag
Ag
Ag
Ag
0.50 1.00 1.50 2.00 2.50 3.00 3.50 4.00 4.50 5.00 keV
B
c:\edax32\genesis\genspc.spc
Label:
kV:20.0 Tilt:0.1 Take-off:34.9 Det: SDD Apollo 40
Res:125 Amp.T:6.40 FS:4431 Lsec:22 5-Oct-2018 10:45:20
C
O
N
S
0.60 1.20 1.80 2.40 3.00 3.60 4.20 4.80 5.40 6.00 keV
C
(a)
D
(b)
E
SE1
C K
N K
O K
S K
AgL
C N O S Ag
50µm
F
SE1
C K
N K
O K
S K
C N O S
50µm

however, the pores were observed to be more amorphous and sequential in this study because of the existence of silver ions [9, 12–17]. However, structures with pores were observed in both of the metal ions used.

## Electrical analysis

The dielectric constant of the samples was measured as a function of the frequency of the applied electric field at room temperatures. The investigation of dielectric spectroscopies such as $\varepsilon'$, $\varepsilon''$ and tan$\delta$ the real and imaginary parts of electric modulus ($M'$ and $M''$) of molecular imprinting and non-imprinting cryogels have been studied via impedance spectroscopy by varying frequency from 1 Hz–10 MHz at 300 K. Materials preferred for dielectric measurements should have important qualities such as good dielectric properties and electric modulus. All of these parameters were obtained by using the following formulas.

$$\varepsilon^* = \varepsilon' - j\varepsilon'' \tag{1}$$

$$\tan\delta = \frac{\varepsilon''}{\varepsilon'} \tag{2}$$

$$M^* = \frac{1}{\varepsilon^*} = M' + jM'' = \frac{\varepsilon'}{\varepsilon'^2 + \varepsilon''^2} + j\frac{\varepsilon''}{\varepsilon'^2 + \varepsilon''^2} \tag{3}$$

$$Z = \frac{1}{2\pi f C_0}\left[\frac{\varepsilon}{\varepsilon'^2 + \varepsilon''^2}\right]; Z = \frac{1}{2\pi f C_0}\left[\frac{\varepsilon}{\varepsilon'^2 + \varepsilon''^2}\right] \tag{4}$$

Here, $\varepsilon'$ and $\varepsilon''$ are the real and the imaginary parts of complex dielectric permittivity; $M'$ and $M''$ are real and imaginary parts of electric modulus; $Z'$ and $Z''$ are real and imaginary impedance and tan$\delta$ is loss factor of dielectric permittivity.

Figures 4 and 5 illustrate the real (dielectric constant) and imaginary (dielectric loss) parts of the permittivity of a molecular imprinting and non-imprinting cryogel,

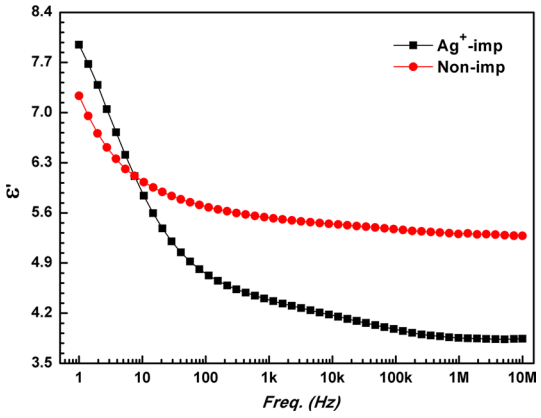


**Fig. 4** Real part of dielectric permittivity of cryogel samples at room temperatures

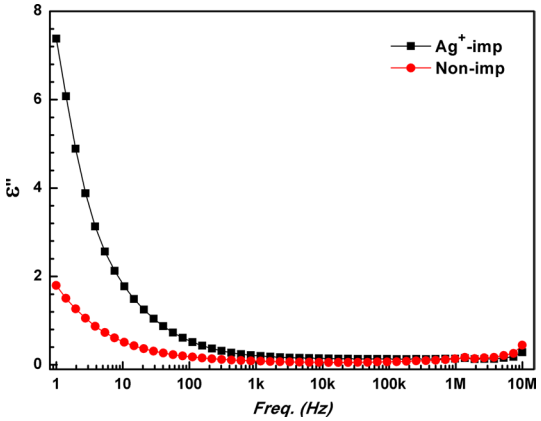


**Fig. 5** Imaginary part of dielectric permittivity of cryogel samples at room temperatures

respectively. The samples should be analyzed very well in terms of dielectric properties to examine the conductivity behavior in $Ag^+$-imprinted and non-imprinted supermacroporous cryogels polymeric materials. The decrease in the dielectric constant of $Ag^+$-imprinted cryogels especially at high frequencies can be attributed to the increase in the number of charges carriers caused by $Ag^+$ [46, 47]. It is physically important that the amount of dielectric loss in the characteristic behavior of Fig. 5 is approximately four times higher in the $Ag^+$-imprinted cryogel. The four times higher dielectric loss rate in $Ag^+$-imprinted cryogel than non-imprinted cryogel can be ascribed to the additional contribution to conductivity as a result of the imprinted silver ions with the cryogel [48, 49]. As seen in Figs. 4 and 5, the real part of the permittivity increases at low frequencies as electrode effects become dominant. It shows a constant value at high frequencies due to dipole polarization. At room temperatures, the imaginary part does not show a relaxation peak as the relaxation time of samples is very short [50, 51]. Figures 4 and 5 show a few similar features. First, both the real and imaginary parts of the permittivity decrease when the frequency rises. When frequency decreases, the kinetic energy of the cryogel molecules also decreases proportionally to the frequency while the permittivity of cryogel increases. Both effects reduce the motion of the dipoles in the cryogel. This leads to the reduction in both the real and imaginary parts of the permittivity. The reduction in dielectric permittivity with increasing frequency can be explained by considering time available for the molecular dipoles to follow the field. At low frequencies, the dipoles have sufficient time to follow and align with the field, resulting in larger values of the permittivity [52, 53]. Besides that, the rise seen in the real part of the permittivity at lower frequency in Fig. 4 is due to dipole polarization. Though we expect the plateau at high frequencies, there is also a weak plateau at low (intermediate) frequencies, indicating the presence of relaxation processes at different frequencies at room temperatures.

The three major features noticed in cryogel samples can also be seen in Figs. 4 and 5. There are decreases in both parts of the permittivity with increasing frequency. Since the cryogel contains 88% water, the explanations for these features are the same as in water. The dielectric loss peak is not clearly visible due to the

complexity of the material compared to the ideal Debye material. In addition to these features, Fig. 4 shows more than one bump in $\varepsilon'$ as a function of frequency. This is an indication of the presence of more than one relaxation process in these cryogel samples.

The ratio of the imaginary part of the permittivity to the real part gives the dielectric loss tangent, tan$\delta$. Comparative plots of the loss tangent tan$\delta$ in the molecular imprinting and non-imprinting cryogels in wide range of frequency (from 10 Hz to 10 MHz) are shown in Fig. 6. In addition that is precisely in suitable of tangent characteristics with the results of morphological SEM image and impedance properties. So, the loss tangent behavior can be employed as a favored technique to determine structural properties of the materials. In order to obtain more detail in determining the structure of both $Ag^+$-imprinted cryogel and $Ag^+$-non-imprinted cryogel, the loss tangent behaviors were examined at different frequencies [54]. Measurements of the loss tangent indicate the presence of relaxation processes in the all cryogels. This relaxation process was similar to the process observed in water dielectric. Similar to water, the relaxation peaks in the loss tangent move to lower frequency due to a slowing of the relaxation processes. As can be seen from Fig. 6, the values of tan$\delta$ decrease exponentially as the frequency increases at a wide frequencies range of 10 Hz–10 MHz. On the other hand, these values keep almost constant at a highest frequency range of 10 kHz–10 MHz. An increase in frequency is accompanied by flaws in the lattice as well as the moving capacity of ions and electrons [55–61]. Those curves are quite similar to the ones suggested by Debye relaxation model for orientational polarization [62].

Complex modulus analysis can be used as another way of investigating the electrical features of the sample, rendering it as a sought-after means of identifying, analyzing and understanding the dynamical features in the concept of electric transport (i.e., parameters such as carrier/ion hopping rate, conductivity relaxation time). In the analysis and interpretation of the data obtained in the experiments, model equivalent circuit supplying the exact signification of the electrical qualities is of great importance. This modulus signification represses the negative

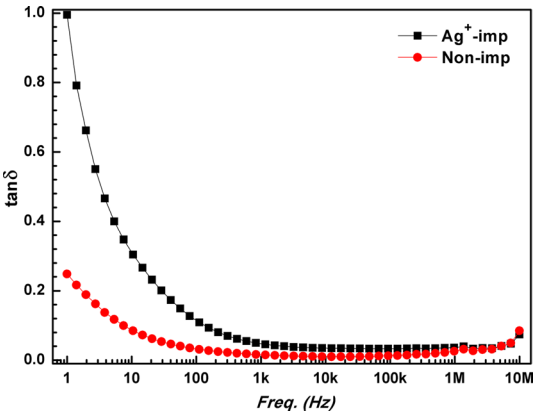


**Fig. 6** Dielectric loss tangent factor of cryogel samples at room temperatures

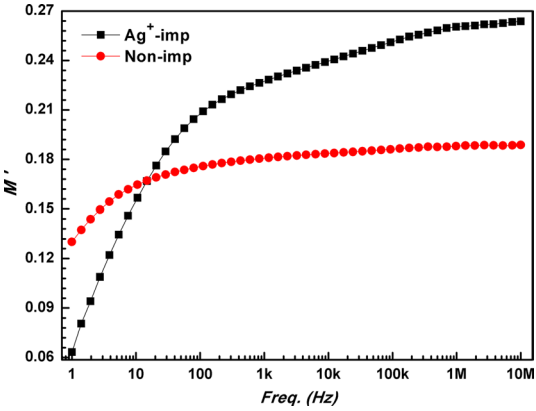


**Fig. 7** Real part of the complex electric modulus of cryogel samples at room temperatures

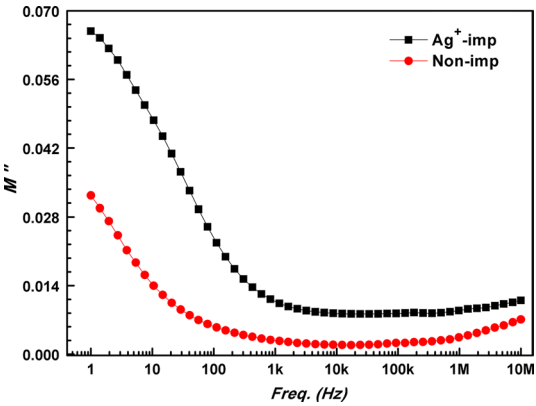


**Fig. 8** Imaginary part of the complex electric modulus of cryogel samples at room temperatures

impacts of extrinsic relaxation which is generally employed in analyzing dynamic conductivities of ionically conducting glasses.

The dielectric modulus ($M^* = 1/\varepsilon^*$) is generally employed in analyzing dielectric data [63, 64]. The benefit in using complex electric modulus spectra stems from the fact that it can be used in differentiating between electrode polarization and grain boundary conduction process. The application of electric modulus spectroscopic analysis facilitates building a relationship between this concept and other features, particularly the dynamical mechanical modulus. Figure 7 shows the frequency dependence of real part ($M'$) complex electric modulus ($M^*$) for cryogel samples whose frequency may stand somewhere between 1 Hz and 10 MHz. It can be seen from the figure that $M'(f)$ values tend closer to zero with decreasing frequency and increase exponentially with increasing frequency. This shows that electrode polarization is of low levels in the samples [65].

Figure 8 shows the frequency dependence of imaginary part ($M''$) complex electric modulus ($M^*$) for cryogel samples whose frequency may stand somewhere between 1 Hz and 10 MHz. The plots of $M''$ ($f$), as shown in Fig. 8, exhibit the

increase for $M''$ at low frequencies between 1 Hz and 1 kHz. At frequencies above $f_{max}$, the carriers are mobile on short distances because they are confined to their potential wells, pointing to fact that the dielectric relaxation is not the usual frequency activated type dominated by hopping mechanism of charge carriers. The dielectric relaxation mechanism is activated with a lower frequency. It is through the modulus spectra that dipole mechanism can be proven to have a role in transmitting electricity in the materials [66].

Figure 9 exhibits the impedance curves of $Ag^+$-imprinting and non-imprinting samples. Besides the incomplete semi-circle in both $Ag^+$ imprinted cryogel and $Ag^+$ non-imprinted cryogel, almost no semi-circular tendency was observed as the frequency increased, and for the relaxation mechanism it could be said to be dominant only at low frequency. Namely; impedance characteristics exhibit the non-Debye behavior [67, 68]. Besides that, the semicircular diameters of the silver ion-imprinted cryogel sample tend to increase. This is due to the reduction in conductivity caused by silver ions deficiency in non-imprinted cryogel samples [54]. Besides the incomplete semicircle in both $Ag^+$-imprinted cryogel and $Ag^+$-non-imprinted cryogel, almost no semicircular tendency was observed as the frequency increased and so the relaxation mechanism could be said to be dominant only at low frequency. It is well known that the cryogel materials can be modified for their electrical and dielectric properties due to the fact that both ion-imprinted and non-imprinted [54] cryogels can be obtained.

## Conclusion

Cryogels and their physical properties are very interesting topics in the literature due to their application in the biotechnology. This was the motivation for the present work. Therefore, a novel ion-imprinting and non-imprinting cryogel samples have been prepared using ion-imprinting technique and the dielectric properties using an impedance spectroscopy method have been investigated. In the preparation of ion-imprinted cryogel, at the first attempt, *N*-methacryloly-(L)-cysteine methyl ester

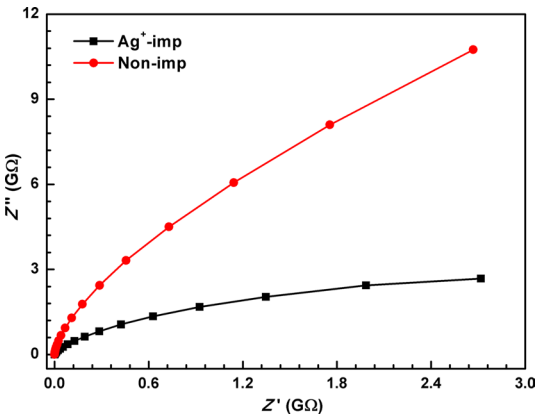


**Fig. 9** Impedance plots (imaginary part versus real part) of cryogel samples at room temperatures

(MAC) was decided to be employed as the metal complexing monomer. It was with the use of bulk polymerization that $Ag^+$-imprinted poly(hydroxyethyl methacrylate-*N*-methacryloly-(L)-cysteine methyl ester) cryogel was obtained. Features such as high chemical and mechanical stability were taken into consideration in determining poly(2-hydroxyethyl methacrylate) (PHEMA) as the fundamental material. Upon removing the template (silver ions), the $Ag^+$-imprinted cryogel was prepared to use as chromatographic column with a view to remove silver ions from silver ion-containing photo-film materials. The dielectric properties of cryogel samples have been studied through impedance spectroscopy, the frequency range of which was 1 Hz–10 MHz. The real part of the permittivity increases at low frequencies as electrode effects become dominant. It shows a constant value at high frequencies due to dipole polarization. On the other hand, the imaginary part does not show a relaxation peak as the relaxation time of samples is very short. The basic features noticed in cryogel samples in terms of dielectric measurements can be shown easily by decreasing both parts of the permittivity with increasing frequency, containing high volume water of cryogel due to the fact that they nearly have same properties as the water. Electrical features of material can be investigated through complex modulus analysis, which can be considered as another viable method. In identifying analysis and coming up with a sound understanding of dynamical aspect of electrical transport, this modulus analysis is of great significance and convenience. In coming up with the result of the data obtained through experiments, using a model equivalent circuit is necessary on grounds that this truly signifies the electrical features. For this, the frequency dependence of electrical modulus has also been investigated. The experimental data exhibited that the real part of electrical modulus ($M'$ ($f$)) is indicative of negligible electrode polarization phenomenon in the test material. The behavior of the imaginary part of the electrical modulus ($M''$ ($f$)) applied frequency consist that the dielectric relaxation is not the usual frequency activated type dominated by hopping mechanism of charge carriers. It is through the modulus spectra that dipole mechanism can be proven to have a role in transmitting electricity in the materials. As the result, ion-imprinted cryogels have great importance on the removal of heavy metal ions from industrial waste waters and aqueous solutions. Besides that, the dielectric properties of silver ion-imprinted cryogel show that they can be applied as an insulator material on electronic device applications. Cryogels should be considered as promising material on their future applications such as organic field-effect transistor (OFET), capacitor or supercapacitor and diode because of physical properties of these materials.

**Acknowledgements** Authors thank Prof. Adil Denizli for his support with his facilities during experimental studies and experiences.

## References

1. Ramstrom O, Mosbach K (1999) Synthesis and catalysis by molecularly imprinted materials. Curr Opin Chem Biol 3:759–764
2. Rao T, Daniel TP, Gladis JM (2004) Tailored materials for preconcentration or separation of metals by ion-imprinted polymers for solid-phase extraction (IIP-SPE). Trends Anal Chem 23:28–35

3. Mosbach K, Ramström O (1996) The emerging technique of molecular imprinting and its future impact on biotechnology. Nat Biotechnol 14:163–170
4. Wackerling J, Lieberzeit AP (2015) Molecularly imprinted polymer nanoparticles in chemical sensing—synthesis, characterisation and application. Sens Actuators B Chem 207:144–157
5. Demirel G, Ozcetin G, Turan E, Caykara T (2005) pH/temperature–sensitive imprinted ionic poly(*N*-tert-butylacrylamide-co-acrylamide/maleic acid) hydrogels for bovine serum albumin. Macromol Biosci 5:1032–1037
6. Shiomi T, Matsui M, Mizukami F, Sakaguchi K (2005) A method for the molecular imprinting of hemoglobin on silica surfaces using silanes. Biomaterials 27:5564–5571
7. Wei S, Mizaikoff B (2007) Binding site characteristics of 17β-estradiol imprinted polymers. Biosens Bioelectr 23:201–209
8. Li Y, Yang HH, You QH, Zhuang ZX, Wang XR (2006) Protein recognition via surface molecularly imprinted polymer nanowires. Anal Chem 78:317–320
9. Perçin I, Sener G, Demirçelik AH, Bereli N, Denizli A (2015) Comparison of two different reactive dye immobilized poly(hydroxyethyl methacrylate) cryogel discs for purification of lysozyme. Appl Biochem Biotechnol 175:2795–2805
10. Haginaka J (2008) Monodispersed, molecularly imprinted polymers as affinity-based chromatography media. J Chromatogr B 866:3–13
11. Say R, Birlik E, Ersöz A, Yilmaz F, Gedikbey T, Denizli A (2003) Preconcentration of copper on ion-selective imprinted polymer microbeads. Anal Chim Acta 480:251–258
12. Say R, Ersoz A, Denizli A (2003) Selective separation of uranium containing glutamic acid molecular-imprinted polymeric microbeads. Sep Sci Technol 38:3431–3447
13. Andac M, Say R, Denizli A (2004) Molecular recognition based cadmium removal from human plasma. J Chromatogr B 811:119–126
14. Ersoz A, Say R, Denizli A (2004) Ni (II) ion-imprinted solid-phase extraction and preconcentration in aqueous solutions by packed-bed columns. Anal Chim Acta 502:91–97
15. Yavuz H, Say R, Denizli A (2005) Iron removal from human plasma based on molecular recognition using imprinted beads. Mater Sci Eng C 25:521–528
16. Ersoz A, Denizli A, Ozcan A, Say R (2005) Molecularly imprinted ligand-exchange recognition assay of glucose by quartz crystal microbalance. Biosens Bioelectr 20:2197–2202
17. Pang X, Cheng G, Lu S, Tang E (2006) Synthesis of polyacrylamide gel beads with electrostatic functional groups for the molecular imprinting of bovine serum albumin. Anal Bioanal Chem 384:225–230
18. Lozinsky VI, Plieva FM, Galaev IY, Mattiasson B (2002) The potential of polymeric cryogels in bioseparation. Bioseparation. 10:163–188
19. Çavuş A, Baysal Z, Alkan H (2013) Preparation of poly(hydroxyethyl methacrylate) cryogels containing L-histidine for insulin recognition. Colloids Surf B 107:84–89
20. Thompson T, Fawell J, Kunikane S, Jackson D, Appleyard S, Callan P, Bartram J, Kingston P (2007) Chemical safety of drinking-water: assessing priorities for risk management. World Health Organization Press, Geneva
21. Pedroso MS, Pinho GLL, Rodrigues SC, Bianchini A (2007) Mechanism of acute silver toxicity in the euryhaline copepod *Acartia tonsa*. Aquat Toxicol 82:173–180
22. Mack C, Wilhelmi B, Duncan JR, Burgess JE (2007) Research review paper: biosorption of precious metals. Biotechnol Adv 25:264–271
23. US Environmental Protection Agency (1999) National Recommended Water Quality Criteria-Correction, EPA-822-Z-99-001. Office of Water, Washington
24. Arvidsson P, Plieva FM, Savina IN, Lozinsky VI, Fexby S, Bülow L, Galaev IY, Mattiasson B (2002) Chromatography of microbial cells using continuous supermacroporous affinity and ion-exchange columns. J Chromatogr A 977:27–38
25. Kumar A, Plieva FM, Galaev IY, Mattiasson B (2003) Affinity fractionation of lymphocytes using a monolithic cryogel. J Immunol Methods 283:185–194
26. Yao KJ, Yun JX, Shen SC, Wang LH, He XJ, Yu XM (2006) Characterization of a novel continuous supermacroporous monolithic cryogel embedded with nanoparticles for protein chromatography. J Chromatogr A 1109:103–110
27. Mafu LD, Msagati TA, Mamba BB (2013) Ion-imprinted polymers for environmental monitoring of inorganic pollutants: synthesis, characterization, and applications. Environ Sci Pollut Res Int 20(2):790–802

28. Yoshikawa M (2008) Surface plasmon resonance studies on molecularly imprinted films. J Polym Appl Sci 110:2826–2832
29. Haginaka J (2001) HPLC-based bioseparations using molecularly imprinted polymers. Bioseparation 10:337–351
30. Ye L, Mosbach K (2001) Polymers recognizing biomolecules based on a combination of molecular imprinting and proximity scintillation: a new sensor concept. J Am Chem Soc 123:2901–2902
31. Zhang L, Cheng G, Fu C (2003) Synthesis and characteristics of tyrosine imprinted beads via suspension polymerization. React Funct Polym 56:167–173
32. Nicholl IA, Rosengren JP (2001) Molecular imprinting of surfaces. Bioseparation 10:301–305
33. Cormak PAG, Mosbach K (1999) Molecular imprinting: recent developments and the road ahead. React Funct Polym 41:115–124
34. Kyritsis A, Pissis P, Grammatikakis J (1995) Dielectric relaxation spectroscopy in poly(hydroxyethyl acrylates)/water hydrogels. J Polym Sci Part B Polym Phys 33(12):1737–1750
35. Aziz SB, Abidin ZHZ, Arof AK (2010) Influence of silver ion reduction on electrical modulus parameters of solid polymer electrolyte based on chitosansilver triflate electrolyte membrane. Express Polym Lett. https://doi.org/10.3144/expresspolymlett.2010.38
36. Aziz SB (2017) Investigation of metallic silver nanoparticles through UV–Vis and optical micrograph techniques. Int J Electrochem Sci 10:363–373
37. Aziz SB, Abidin ZHZ, Arof AK (2010) Effect of silver nanoparticles on the DC conductivity in chitosan-silver triflate polymer electrolyte. Phys B Phys Condens Matter 405:4429–4433. https://doi.org/10.1016/j.physb.2010.08.008
38. Aziz SB, Abidin ZHZ (2014) Electrical and morphological analysis of chitosan: AgTf solid electrolyte. Mater Chem Phys 144:280–286. https://doi.org/10.1016/j.matchemphys.2013.12.029
39. Aziz SB, Abidin ZHZ, Kadir MFZ (2015) Innovative method to avoid the reduction of silver ions to silver nanoparticles ($Ag^{+} \rightarrow Ag^{\circ}$) in silver ion conducting based polymer electrolytes. Phys Scr 90:035808. https://doi.org/10.1088/0031-8949/90/3/035808
40. Aziz SB, Abdullah OG, Rasheed MA (2017) A novel polymer composite with a small optical band gap: new approaches for photonics and optoelectronics. J Appl Polym Sci 134:10. https://doi.org/10.1002/app.44847
41. Aziz S, Abdullah R, Rasheed M et al (2017) Role of ion dissociation on DC conductivity and silver nanoparticle formation in PVA: AgNt based polymer electrolytes: deep insights to ion transport mechanism. Polymers (Basel) 9:338. https://doi.org/10.3390/polym9080338
42. Aziz SB, Rasheed MA, Abidin ZHZ (2017) Optical and electrical characteristics of silver ion conducting nanocomposite solid polymer electrolytes based on chitosan. J Electron Mater 46:6119–6130. https://doi.org/10.1007/s11664-017-5515-8
43. Aziz SB (2017) Morphological and optical characteristics of chitosan$_{(1-x)}$: $Cu^{o}_{x}$ ($4 \leq x \leq 12$) based polymer nano-composites: optical dielectric loss as an alternative method for Tauc's model. Nanomaterials 7:444. https://doi.org/10.3390/nano7120444
44. Aziz S, Abdulwahid R, Rasheed M et al (2017) Polymer blending as a novel approach for tuning the SPR peaks of silver nanoparticles. Polymers (Basel) 9:486. https://doi.org/10.3390/polym9100486
45. Utku S, Yılmaz E, Türkmen D et al (2008) Ion-imprinted thermosensitive polymers for $Fe^{3+}$ removal from human plasma. Hacettepe J Biol Chem 36:291–304
46. Aziz SB, Woo TJ, Kadir MFZ, Ahmed HM (2018) A conceptual review on polymer electrolytes and ion transport models. J Sci Adv Mater Devices 3:1–17. https://doi.org/10.1016/J.JSAMD.2018.01.002
47. Aziz SB (2013) $Li^{+}$ ion conduction mechanism in poly(ε-caprolactone)-based polymer electrolyte. Iran Polym J 22:877–883. https://doi.org/10.1007/s13726-013-0186-7
48. Aziz SB, Abdullah O, Hussein S et al (2017) Effect of PVA blending on structural and ion transport properties of CS: AgNt-based polymer electrolyte membrane. Polymers (Basel) 9:622. https://doi.org/10.3390/polym9110622
49. Aziz SB (2016) Erratum to: Occurrence of electrical percolation threshold and observation of phase transition in chitosan$_{(1-x)}$: $AgI_{x}$ ($0.05 \leq x \leq 0.2$)-based ion-conducting solid polymer composites. Appl Phys A 122:785. https://doi.org/10.1007/s00339-016-0272-8
50. Szu SP, Lin CY (2003) AC impedance studies of copper doped silica glass. Mater Chem Phys 282:295–300
51. Kwok HL, Siu WC (1979) Carrier concentration and mobility in chemically sprayed cadmium sulphide thin films. Thin Solid Films 61:249–257

52. Buchner R, Stauber J, Barthel J (1999) The dielectric relaxation of water between 0 °C and 35 °C. Chem Phys Lett 306:57–63
53. Angulo-Sherman A, Mercado-Uribe H (2014) Water under inner pressure: a dielectric spectroscopy study. Phys Rev E 89:022406(1–5)
54. Aziz SB, Abdullah RM (2018) Crystalline and amorphous phase identification from the tan$\delta$ relaxation peaks and impedance plots in polymer blend electrolytes based on [CS:AgNt]$x$:PEO($x-1$) ($10 \leq x \leq 50$). Electrochim Acta 285:30–46. https://doi.org/10.1016/J.ELECTACTA.2018.07.233
55. Kaatze U (1989) Complex permittivity of water as a function of frequency and temperature. J Chem Eng Data 34:371–374
56. Prabakar K, Narayandass SK, Mangalaraj D (2003) Dielectric properties of $Cd_{0.6}Zn_{0.4}Te$ thin films. Phys Status Solidi A 199:507–514
57. Abdel Kader MM, Elzayat MY, Hammad TR, Aboud AI, Abdelmonem H (2011) Dielectric permittivity, AC conductivity and phase transition in hydroxyl ammonium sulfate. Phys Scr 83:1–7
58. Satter AA, Samy AR (2003) Dielectric properties of rare earth substituted Cu–Zn ferrites. Phys Status Solidi(a) 200:415–422
59. Maurya D, Kumar J (2005) Dielectric-spectroscopic and a.c. conductivity studies on layered $Na_{2-X}K_XTi_3O_7$ (X = 0.2, 0.3, 0.4) ceramics. J Phys Chem Solids 66:1614–1620
60. Maity S, Bhattacharya D, Ray SK (2011) Structural and impedance spectroscopy of pseudo-coablated $(SrBi_2Ta_2O_9)_{(1-x)}$–$(La_{0.67}Sr_{0.33}MnO_3)_x$ composites. J Phys D Appl Phys 44:1–10
61. Matheswaran P, Saravanakumar R, Velumani S (2010) AC and dielectric properties of vacuum evaporated InTe bilayer thin films. Mater Sci Eng B 174:269–272
62. Moynihan CT (1994) Analysis of electrical relaxation in glasses and melts with large concentrations of mobile ions. J Non-Cryst Solids 172–174:1395–1407
63. Moynihan CT, Boesch LP, Laberge NL (1973) Decay function for the electric field relaxation in vitreous ionic conductors. Phys Chem Glasses 14:122–125
64. Sural M, Ghosh A (1998) Electrical conductivity and conductivity relaxation in glasses. J Phys Condens Matter 10:10577–10586
65. Sinclair DC, West AR (1989) Impedance and modulus spectroscopy of semiconducting $BaTiO_3$ showing positive temperature coefficient of resistance. J Appl Phys 66:3850–3856
66. Sinclair DC, West AR (1994) Effect of atmosphere on the PTCR properties of $BaTiO_3$ ceramics. J Mater Sci 29:6061–6068
67. Aziz SB, Karim WO, Qadir K, Zafar Q (2018) Proton ion conducting solid polymer electrolytes based on chitosan incorporated with various amounts of barium titanate ($BaTiO_3$). Int J Electrochem Sci 13:6112–6125. https://doi.org/10.20964/2018.06.38
68. Aziz SB (2018) The Mixed contribution of ionic and electronic carriers to conductivity in chitosan based solid electrolytes mediated by CuNt salt. J Inorg Organomet Polym Mater 28:1942–1952. https://doi.org/10.1007/s10904-018-0862-3


## Affiliations


**Koray Şarkaya[1,3] · Ahmet Demir[2]**

[1] Department of Chemistry, Faculty of Science and Letters, Duzce University, Düzce, Turkey

[2] Department of Physics, Faculty of Arts and Sciences, Düzce University, Düzce, Turkey

[3] Department of Chemistry, Hacettepe University, Ankara, Turkey